Ceramics-Silikáty 69 (2), 288-297 (2025)
www.ceramics-silikaty.cz doi: 10.13168/cs.2025.0013

EFFECT OF THE LOW CALCINATION TEMPERATURE AND MgO CONTENT ON THE FORMATION AND EXPANSION CHARACTERISTICS OF $C_4A_3\$$

HONGLING FAN, RUOXUE HUANG, GUIXIN HUANG, YONGBO HUANG, PENGKUN HOU, PIQI ZHAO, #SHOUDE WANG, XIN CHENG

Shandong Provincial Key Laboratory of Preparation and Measurement of Building Materials, University of Jinan, Jinan 250022, China

#E-mail: 13589047192@163.com

Submitted December 11, 2024; accepted February 24, 2025

Keywords: Magnesium oxide, Calcium sulfoaluminate, Expansion rate, Calcination temperature, Hydration properties

Research of $C_4A_3\$$ modified Portland clinker is a key solution for the low-carbon cement industry with high-magnesium low-grade limestone as a raw material, in which the coexistence of $C_4A_3\$$ and C_3S at low sintering temperature is key. Thus, this study investigated the effect of a low calcination temperature (1200, 1250, 1300, 1350 °C) on the formation of $C_4A_3\$$, as well as the influence of the MgO content (0, 1, 2, 3, 6 %) on the formation of $C_4A_3\$$ and its hydration expansion under different calcination temperatures. X-ray diffraction (XRD) was used to analyse the phase composition and hydration expansion tests were also conducted. The results showed that the use of a lower calcination temperature at longer holding times promoted the formation of $C_4A_3\$$,, where 1250 °C was considered to be the temperature at which $C_4A_3\$$ begins to form at a faster rate. Compared to the formation of $C_4A_3\$$ at the normal calcination temperature (1350 °C), the formation of $C_4A_3\$$ at 1250 °C was only 10 % lower. In the $C_4A_3\$$ phase, MgO exists in an interstitial solid solution form, and the addition of 1 – 2 % MgO enhances the formation of $C_4A_3\$$ and reduces the hydration swelling, but the formation of $C_4A_3\$$ decreases sligtly with a further increase in the MgO content. This study provides technical support for the research of C4A3$ modified Portland clinker using high-magnesium low-grade limestone as the raw material at low calcination temperatures.

INTRODUCTION

Calcium sulfoaluminate-modified Portland clinker has emerged as a crucial building material with significant potential for diverse applications, positioning it as a strategic pathway toward achieving carbon neutrality. Despite its promise, cement production remains a major global source of carbon emissions, emphasising the urgent need for innovative approaches to mitigate its environmental impact. A key strategy in this regard is lowering the calcination temperature, which not only reduces the energy consumption, but also decreases the CO_2 emissions. In this context, low-grade limestone has attracted attention for its ability to lower the thermal decomposition temperature of limestone by approximately 30 – 50 °C, thereby reducing the heat absorption and energy input by 118.6 kJ·mol^{-1}. The naturally occurring MgO in low-grade limestone, primarily in the form of magnesite ($MgCO_3$) or dolomite ($CaMgCO_3$), plays a pivotal role in this process. The MgO content typically ranges from 19 to 22 % in dolomite-rich variants. Substituting traditional high-grade limestone with these MgO-rich low-grade alternatives introduces 1 – 3 % MgO into the raw mix, modifying the decomposition kinetics while maintaining the material performance. This integration of lower calcination temperatures with more sustainable resource utilisation has spurred extensive research into high-magnesium limestone applications, providing a dual advantage of decarbonisation and cost efficiency for next-generation cement technologies [1, 2].

However, in practical applications, ensuring the strength stability and performance optimisation of low-grade high-magnesium limestone cement remains one of the core challenges for technological breakthroughs [3, 4]. In particular, the influence of magnesium oxide (MgO) on the formation and hydration process of $C_4A_3\$$ has become the key to solving this bottleneck. An in-depth study of this influence mechanism can provide a more reliable technical guarantee for the production of low-carbon cement and new solutions for the optimisation of sustainable building materials [5, 6].

In $C_4A_3\$$-modified Portland clinkers, sintering temperature is one of the key factors affecting the formation of $C_4A_3\$$. It has been shown that the sintering temperature has a significant effect on the formation of $C_4A_3\$$ as well as its hydration characteristics [7, 8]. At low sintering temperature, the reaction between aluminates and sulfates is incomplete, leading to decrease in the $C_4A_3\$$ content, which directly affects the early strength and mechanical properties of the cement [9]. In contrast, a higher sintering temperature can promote the formation of the $C_4A_3\$$ phase and improve its structural stability, thus enhancing the strength and durability of the cement [10-12]. However, a sintering temperature that is too high may generate excessive quartz phases or other unfavourable silicate phases, thus affecting the microstructure and properties of the cement [13]. Therefore, optimising the sintering temperature to ensure the stable formation of $C_4A_3\$$ phase is the key to improving the performance of cement [14].

The role of magnesium oxide (MgO) in $C_4A_3\$$--modified Portland clinkers, especially in the production of cements based on low-grade, high-magnesium limestone as raw material, has become a focus of research [15, 16]. MgO not only affects the formation of $C_4A_3\$$, but also has a significant effect on the hydration expansion rate of the cement [17-19]. The reaction of MgO with sulfate in the cement produces magnesium aluminates (e.g., $4CaO\text{-}MgO\text{-}Al_2O_3\text{-}xH_2O$), and this reaction changes the hydration characteristics and microstructure of the cement [20, 21]. A moderate amount of MgO helps to improve the resistance of cement to sulfate attack and positively affects the early strength of cement [22, 23]. However, when the MgO content is too high, the hydration expansion of magnesium aluminates can lead to volume expansion of the cement and cracks, thus affecting the long-term stability and mechanical properties of the cement [24-26]. Excess MgO may also interfere with the stability of $C_4A_3\$$, increasing the risk of shrinkage and swelling of the cement [27]. Therefore, optimising the content of MgO and its interaction with other components is the key to solving the problem of cement hydration and expansion.

The present study aimed to experimentally investigate the formation of $C_4A_3\$$ and the changes in its properties under different sintering conditions and to further assess the feasibility of low-carbon cement production. The study used lower sintering temperatures (1200, 1250 °C) and different holding times (30, 60, 90, 120 min) as the experimental variables and a common sintering temperature (1350 °C) as a control to analyse the formation characteristics of $C_4A_3\$$ and its effect on cement properties under low temperature conditions. At the same time, the study also investigated the role of magnesium oxide (MgO) in regulating the amount of $C_4A_3\$$ formation and its hydration expansion rate at different sintering temperature and holding times. By optimising the ratio of low sintering temperature and appropriate amount of MgO, this study not only provides technical support for the production of cement with high magnesium and low-grade limestone as raw material but also provides a theoretical basis for improving the performance of low-calcium cement in construction, thus promoting the application and development of decarbonised cement.

EXPERIMENTAL

Specimen preparation

The chemical reagents used in this study - magnesium oxide (MgO), calcium carbonate, gypsum ($CaSO_4 \cdot 2H_2O$), and aluminium oxide (Al_2O_3) - were sourced from China National Pharmaceutical Group Chemical Reagents Co., Ltd. The MgO contents in the specimens were set at 0, 1, 2, 3 and 6 %. Each raw material was precisely weighed according to the specified proportions and added to a mixing vessel [28, 29]. The mixture was then thoroughly blended in a rotary drum mixer for two hours [29]. After mixing, a precise amount of water was added to form a homogeneous paste, which was compacted into discs with a diameter of 60 mm and a thickness of 8 mm. These discs were placed in a drying oven and heated at 60 °C for two hours to ensure complete drying and eliminate any residual moisture [30, 31].

The prepared discs were then sintered in a high temperature furnace and based on the heating rate of 10 $°C \cdot min^{-1}$, the time needed to reach 1200 °C from 20 °C is 118 min, while the time to reach 1250 °C is 123 min, 1300 °C is 128 min, and 1350 °C is 133 min. Compared to 1200 °C (as the initial temperature), these samples are longer exposed to temperatures than the holding times of 30, 60, 90, and 120 min and then cooled rapidly in the air to obtain the final clinker [29, 32]. The cooled samples were then ground into a fine powder using an agate mortar and subsequently sieved through a 0.074 mm mesh sieve for use in the subsequent tests [28].

Testing methods

Phase composition analysis

Approximately two grams of the calcined clinker was finely ground in an agate mortar until a smooth, particle-free powder was achieved. The resulting sample was analysed using a Bruker D8 A25x X-ray diffractometer (XRD) to determine its mineralogical composition [31]. The XRD measurements were performed under the following conditions: copper target, tube voltage of 40 kV, tube current of 40 mA, scan speed of 0.12 seconds per step, step size of 0.02° and a scanning range (2θ) of 5° to 70° [33]. The PSD calibration size was set to 3.3 [34].

Hydration expansion rate test

Assuming the complete conversion of $C_4A_3\$$ to AFt, the following reaction was considered [35].

$$3C_4A_3\$ + 2CaSO_4{\cdot}2H_2O + 34H_2O \rightarrow \rightarrow C_3A{\cdot}3CaSO_4{\cdot}32H_2O + 2Al(OH)_3 \quad (1)$$

$$4CaO{\cdot}3Al_2O_3{\cdot}SO_3 + 2CaO{\cdot}SO_3{\cdot}2H_2O + 34H_2O \rightarrow \rightarrow 3CaO{\cdot}Al_2O_3{\cdot}3CaO{\cdot}SO_3{\cdot}32H_2O + 2Al_2O_3{\cdot}3H_2O \quad (2)$$

In accordance with the JC/T 313-2009 standard, the synthesised $C_4A_3\$$ phase with various MgO contents was uniformly mixed with gypsum ($CaSO_4{\cdot}2H_2O$) in a molar ratio of 1:2. The mixture was then prepared with a water-to-cement ratio of 0.3 and cast into moulds with dimensions of 25 × 25 × 280 mm. After one day, the specimens were demoulded, and their length was measured. Further length measurements were taken at different curing ages to calculate the hydration expansion rate of the samples over time.

RESULTS AND DISCUSSION

Evolution of phase composition in $C_4A_3\$$ single mineral

XRD analysis at 1200 °C

Figure 1 shows the X-ray diffraction (XRD) spectra of the $C_4A_3\$$ phase with various MgO contents, after sintering at 1200 °C for different holding times. By combining the XRD results with quantitative analysis using Topas software, the amounts of $C_4A_3\$$ formation and the content of f-MgO were systematically compared, as summarised in Table 1. The XRD patterns clearly reveal that the primary mineral phases after sintering are $CaSO_4$ and f-CaO, accompanied by trace amounts of intermediate products such as CA and CA_2. With an increase in the holding time, a slight enhancement in the formation of $C_4A_3\$$ was observed. Notably, the diffraction peaks corresponding to $C_4A_3\$$ in the 1 % MgO sample calcined at 1200 °C for 120 min were distinctly pronounced, indicating that $C_4A_3\$$ had formed to a relatively high degree.

However, despite the observed increase in the $C_4A_3\$$ formation with the extended holding time, it is evident that 1200 °C remains a relatively low sintering temperature for the optimal $C_4A_3\$$ synthesis. Thus, although extending the holding time at 1200 °C can enhance the $C_4A_3\$$ formation to some extent, this effect is ultimately limited, suggesting that further optimisation of the sintering process would require an increase in temperature to achieve more substantial $C_4A_3\$$.

Regarding the f-MgO content, a significant reduction in f-MgO was observed in the lower MgO content samples post-sintering. In the samples with 1, 2 and 3 % MgO, the f-MgO content decreased as the holding time increased. This trend suggests that, at lower MgO concentrations, some of the f-MgO likely reacts with other components during sintering, participating in the formation of mineral phases.

In contrast, for the 6 % MgO sample, even after sintering at 1200 °C for 120 min, a distinct peak corresponding to f-MgO remains visible in the XRD pattern. This observation suggests that the solid solution capacity of the Ca-Al oxides for MgO is limited. Notably, the lower MgO content samples exhibited a gradual decrease in f-MgO with the increasing holding time, likely due to the gradual absorption of $CaSO_4$ by intermediate products such as CA and CA_2, which, in turn, facilitated the formation of $C_4A_3\$$. This process may have resulted in the partial incorporation of MgO into the mineral structure. Furthermore, since 1200 °C is a relatively low sintering temperature, the presence of MgO did not significantly influence the formation of $C_4A_3\$$.

XRD analysis at 1250 °C

Figure 2 shows the X-ray diffraction (XRD) patterns of $C_4A_3\$$ single mineral samples sintered at 1250 °C for different holding times and various MgO contents. Table 2 shows the formation of $C_4A_3\$$ and the content of free MgO (f-MgO) in the different samples. Overall, 1250 °C is identified as the temperature at which $C_4A_3\$$ begins to form rapidly. In the production of sulfoaluminate cement, 1250 °C marks the onset of substantial $C_4A_3\$$ formation. When the holding time is 30 min, samples with 0 and 1 % MgO show limited $C_4A_3\$$ formation. A small amount of MgO promotes $C_4A_3\$$ formation, whereas excess MgO inhibits it. As the holding time is extended to 60 min, the amount of $C_4A_3\$$ formed increases considerably. After further

Table 1. $C_4A_3\$$ formation and MgO content at different holding times.

Time (min)	0 % MgO (α %)		1 % MgO (α %)		2 % MgO (α %)		3 % MgO (α %)		6 % MgO (α %)	
	$C_4A_3\$$ %	MgO %	$C_4A_3\$$ %	MgO %	$C_4A_3\$$ %	MgO %	$C_4A_3\$$ %	MgO %	$C_4A_3\$$ %	MgO %
30	1.6	0	1.15	0.98	0.78	1.06	1.06	2.55	0.91	5.36
60	5.54	0	2.19	0.92	1.41	1.28	2.16	2.2	1.26	4.3
90	4.51	0	2.76	0.95	2.38	0.58	1.68	2.17	1.12	4.29
120	3.67	0	9.71	0.56	1.87	0.69	4.85	1.51	2.1	4.37

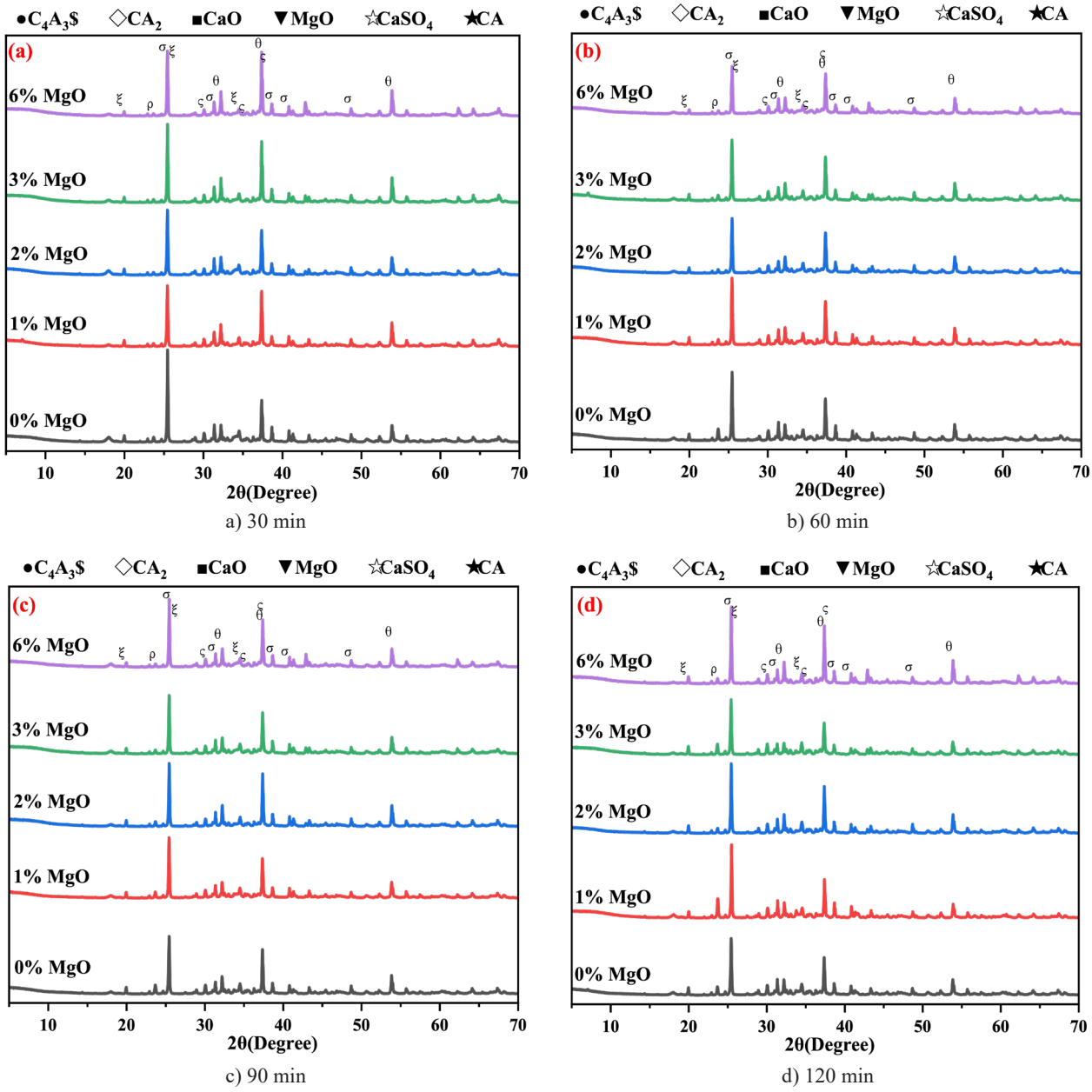

Figure 1. XRD patterns of $C_4A_3\$$ monazite calcined at 1200 °C for holding times of 30, 60, 90, 120 min.

extending the holding time to 90 min, a significant amount of $C_4A_3\$$ is produced and nearly all $CaSO_4$ is consumed.The sample with 1 % MgO exhibits the highest rate of $C_4A_3\$$ formation, while the sample with 6 % MgO shows the lowest rate.

After sintering at 1250 °C for 120 min, all the samples with various MgO contents show substantial $C_4A_3\$$ formation. However, the diffraction peak of $CaSO_4$ remains visible in the XRD patterns. Specifically, the sample with 1 % MgO exhibits the smallest

Table 2. $C_4A_3\$$ formation and MgO content at different holding times.

Time (min)	0 % MgO (α %)		1 % MgO (α %)		2 % MgO (α %)		3 % MgO (α %)		6 % MgO (α %)	
	$C_4A_3\$$ %	MgO %	$C_4A_3\$$ %	MgO %	$C_4A_3\$$ %	MgO %	$C_4A_3\$$ %	MgO %	$C_4A_3\$$ %	MgO %
30	11.33	0	31.43	0.51	5.56	0.66	3.45	1.63	3.78	3.69
60	33.2	0	41.79	0.67	32.93	0.94	23.7	2.77	14.3	4.51
90	47.3	0	72.6	0.62	55.23	1.03	43.6	2.34	40.65	3.91
120	71.15	0	79.58	0.43	74.91	1.07	63.37	2.39	63.39	5.26

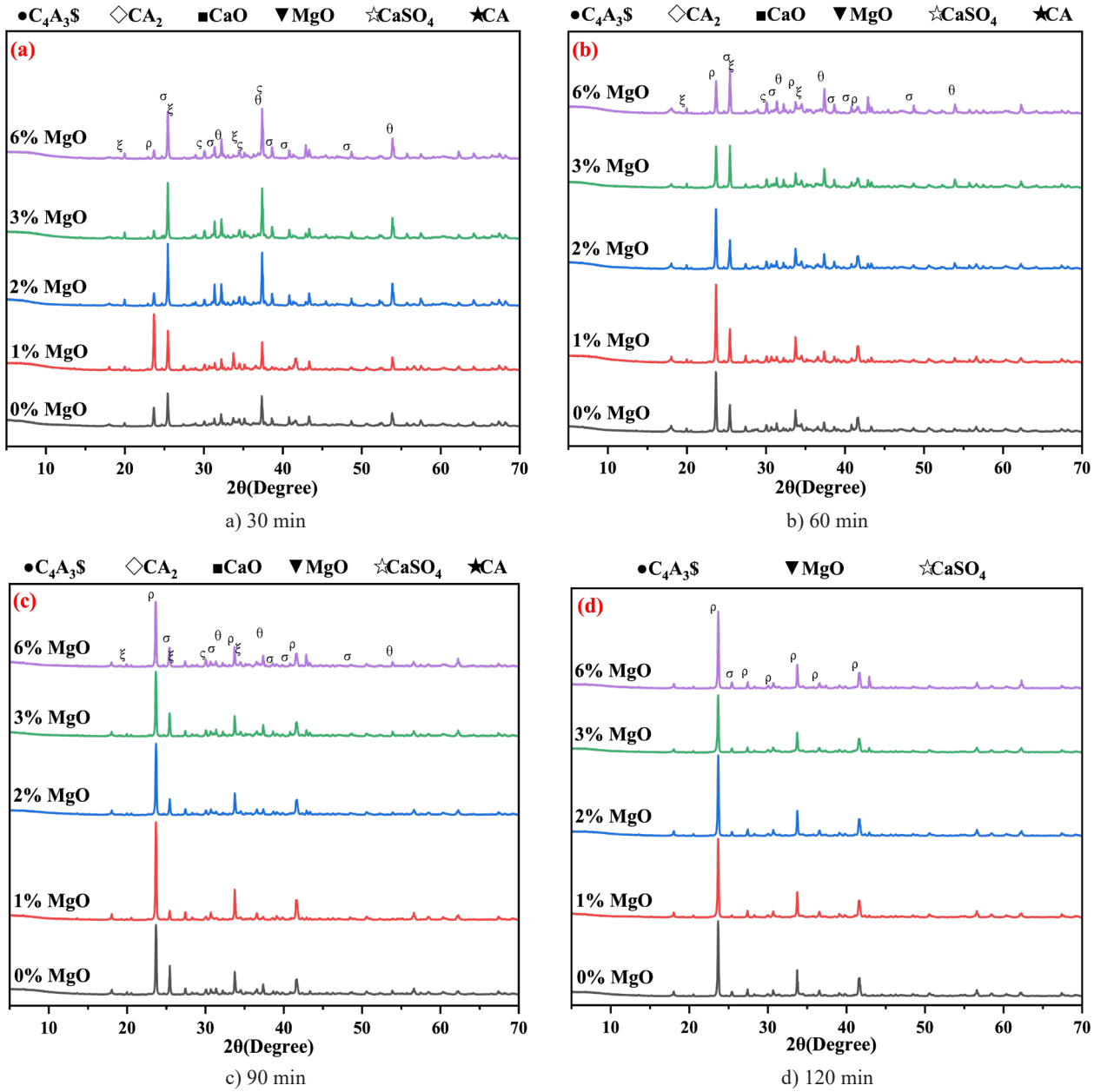

Figure 2. XRD patterns of $C_4A_3\$$ monazite calcined at 1250 °C for holding times of 30, 60, 90, 120 min.

$CaSO_4$ peak, indicating that most $CaSO_4$ has reacted to form $C_4A_3\$$. In contrast, the sample containing 6 % MgO exhibited prominent $CaSO_4$ peaks, suggesting that the conversion of $CaSO_4$ to $C_4A_3\$$ was inhibited at higher MgO concentrations. This implies that an optimal amount of MgO can effectively promote the consumption of $CaSO_4$ and the formation of $C_4A_3\$$, while excess MgO may hinder the reaction. Under the sintering conditions at 1250 °C, the sample with 1 % MgO forms significantly more $C_4A_3\$$ than the samples with other

Table 3. $C_4A_3\$$ formation and MgO content at different holding times.

Time (min)	0 % MgO (α %)		1 % MgO (α %)		2 % MgO (α %)		3 % MgO (α %)		6 % MgO (α %)	
	$C_4A_3\$$ %	MgO %	$C_4A_3\$$ %	MgO %	$C_4A_3\$$ %	MgO %	$C_4A_3\$$ %	MgO %	$C_4A_3\$$ %	MgO %
30	82.19	0	83.35	0.08	85.11	0.61	78.09	1.6	74.36	2.34
60	82.44	0	82.59	0.41	84.1	0.83	80	0.09	74.31	3.56
90	84.24	0	87.05	0.2	85.34	0.89	79.8	1.49	75.93	2.32
120	85.44	0	85.76	0.24	85.34	1.37	78.48	0.72	75.63	1.86

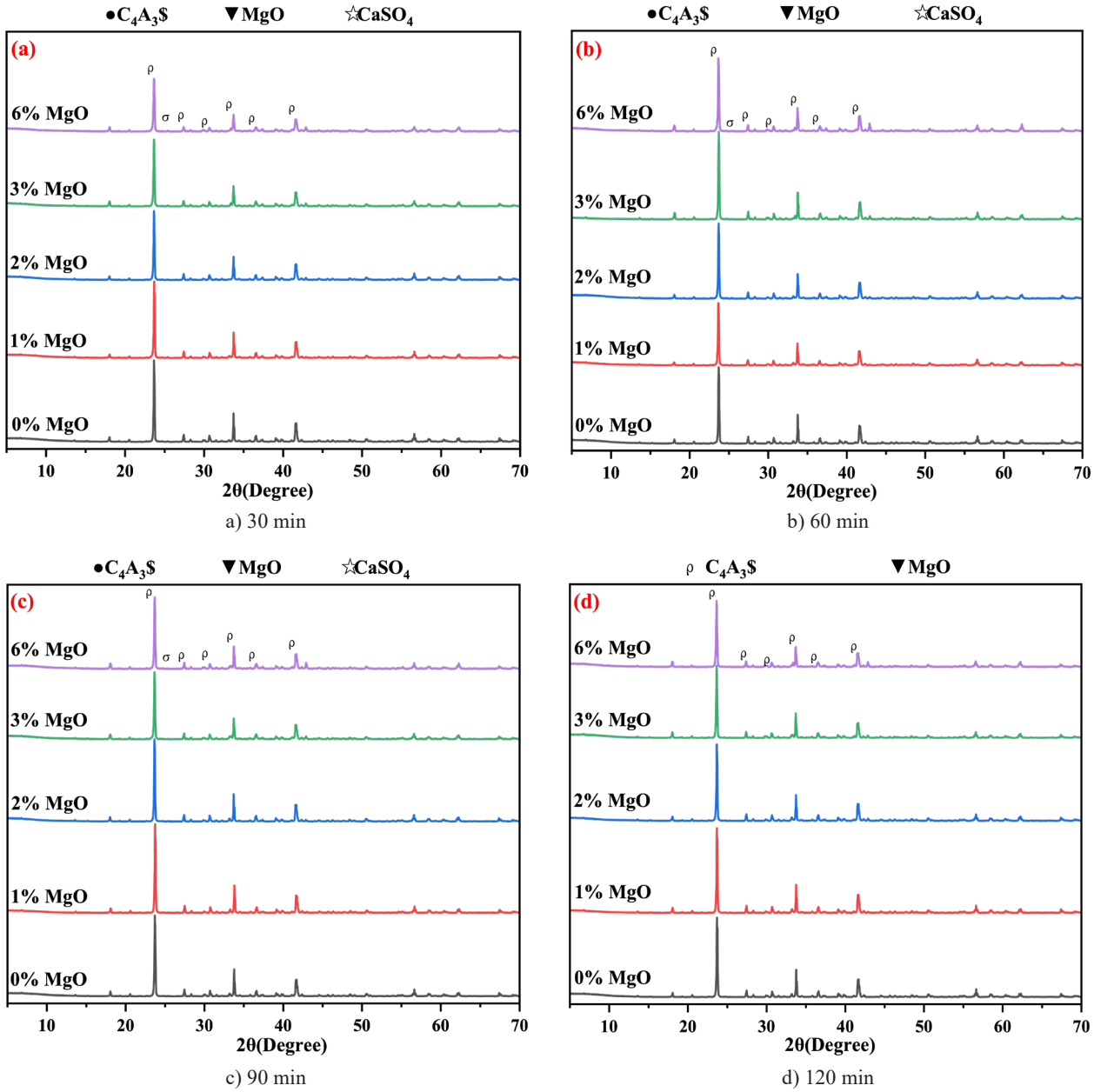

Figure 3. XRD patterns of $C_4A_3\$$ monazite calcined at 1350 °C for holding times of 30, 60, 90, 120 min.

MgO concentrations, indicating that a small amount of MgO is benefit to the $C_4A_3\$$ formation. This promoting effect may manifest at a lower temperature and become more pronounced with longer holding times, providing insights into the optimal MgO content and sintering conditions for $C_4A_3\$$ formation.

XRD analysis at 1350 °C

Figure 3 shows the X-ray diffraction (XRD) patterns of $C_4A_3\$$ phase calcined samples under different holding times and various MgO contents at 1350 °C. As shown in the figure, when calcined at 1350 °C for 30 min, the samples with different MgO contents exhibit the nearly complete formation of $C_4A_3\$$, with almost no diffraction peaks corresponding to the $CaSO_4$ detected. This can be attributed to the fact that 1350 °C is a commonly used sintering temperature for sulphoaluminate cement, which significantly accelerates the synthesis of $C_4A_3\$$. Therefore, even with a relatively short holding time of only 30 min, the formation of $C_4A_3\$$ is rapid, leading to a high synthesis rate. As the holding time increases, the changes in the diffraction peaks of $C_4A_3\$$ become minimal, suggesting that the formation of this mineral is nearly complete.

Table 3 shows the quantitative analysis data of the samples, obtained using Topas software. The data indicate that, compared to samples calcined at lower

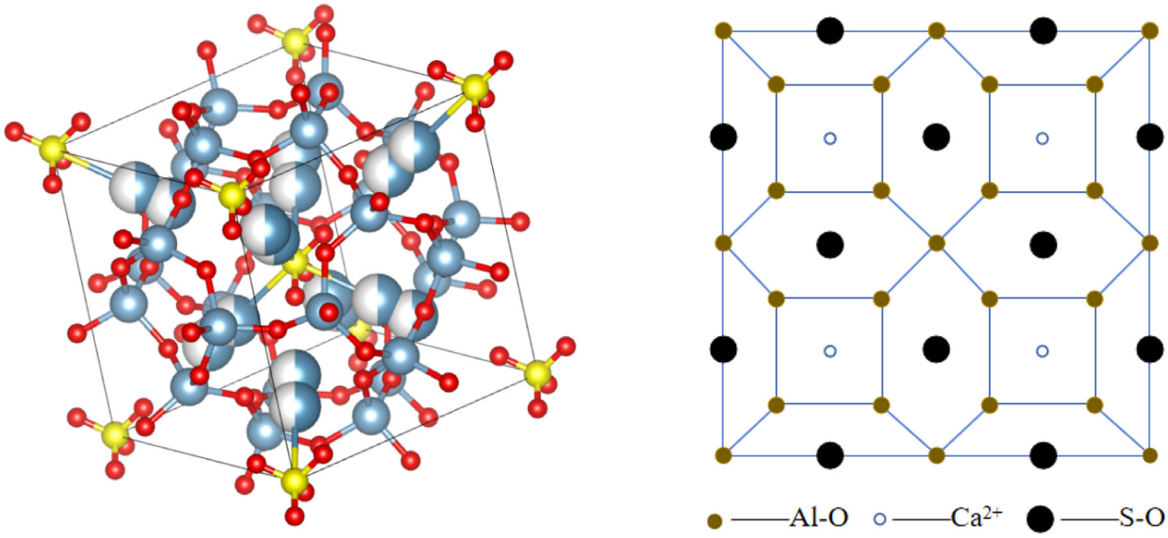

a) 3D structure b) plan view

Figure 4. 3D structure and plan view of $C_4A_3\$$..

temperatures, those at 1350 °C exhibit a reduction in MgO content. Notably, for the $C_4A_3\$$ sample containing 1 % MgO, the amount of free MgO (f-MgO) in the sample calcined at 1350 °C is significantly lower than in the sample calcined at 1250 °C, representing only 15 – 60 % of the f-MgO content in the latter. The formation of $C_4A_3\$$ was only 10 % higher than that at 1250 °C. For the $C_4A_3\$$ with MgO samples calcined at different temperatures, the f-MgO content was generally lower after sintering at 1350 °C. These results suggest that, at 1350 °C, the solubility of MgO in $C_4A_3\$$ significantly increases, leading to a more considerable proportion of MgO being incorporated into the $C_4A_3\$$ structure.

Structural characteristics of $C_4A_3\$$

Figure 4 illustrates the crystal structure of $C_4A_3\$$ with the calcium-oxygen bonds omitted. As depicted in the figure, the crystal structure of $C_4A_3\$$ consists of a porous framework formed by $[AlO_4]$ tetrahedra interconnected at their nodes. Within this framework, four $[AlO_4]$ tetrahedra form square rings, and vertical channels are created along the c-axis. At the $1/4c_0$ and $3/4c_0$ positions along the c-axis, isolated $[SO_4]$ tetrahedra are suspended. At each corner of the square rings formed by the vertical channels, a pair of $[AlO_4]$ tetrahedra are connected, thereby forming rectangular units composed of six $[AlO_4]$ tetrahedra. Calcium ions occupy the rectangular vertical channels along the c-axis, where they are ironically bonded to both the $[AlO_4]$ tetrahedra and $[SO_4]$ tetrahedra. The high reactivity of $C_4A_3\$$is closely associated with this porous structure. This structure, with its large internal cavities, enables $C_4A_3\$$ to incorporate a certain amount of MgO ions through solid solution in the form of interstitial incorporation [36].

The scanning electron microscopy (SEM) analysis of $C_4A_3\$$ reveals an irregular polyhedral crystal morphology with surface-distributed micropores (1 – 5 μm in diameter) and localised particle agglomeration phenomena (Figure 5). The high-magnification imaging demonstrates tightly bonded intergranular interfaces devoid of discernible boundary cracks, indicative of su-perior structural density. Energy-dispersive X-ray spectroscopy (EDS) quantification (Figure 5) identifies primary elemental constituents as Ca (23.74 at. %), Al (18.7 at. %), S (4.67 at. %), and O (50.89 at. %), closely aligned with theoretical stoichiometric proportions (Ca:Al:S:O = 4:6:1:16), thereby confirming the phase purity. These microstructural and compositional characterisations provide critical insights into the swelling behaviour regulation of $C_4A_3\$$ in cementitious matrices.

Effect of MgO on the crystal structure of $C_4A_3\$$

Figure 6 illustrates the effect of MgO on the formation of the $C_4A_3\$$ crystal structure. Samples exhibiting the highest formation of $C_4A_3\$$ (sintered at 1350 °C for 120 min) were selected for the analysis of the resulting $C_4A_3\$$ crystal morphology. As shown in the figure, when the MgO content is less than 2 %, the formation of cubic $C_4A_3\$$ increases with the MgO content, although it remains lower than that of orthorhombic $C_4A_3\$$. This could be attributed to Mg^{2+} ions, acting as dopants, entering the $C_4A_3\$$ lattice and preferentially stabilising the cubic phase, which demonstrates greater tolerance

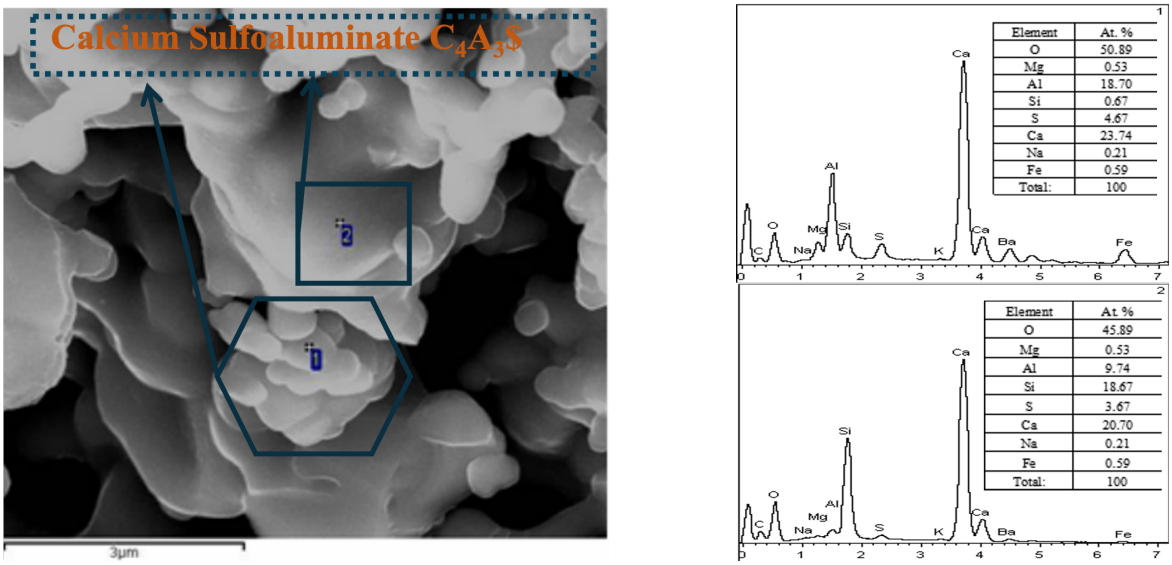

Figure 5. Microscopic morphology (SEM and EDS) of $C_4A_3\$$..

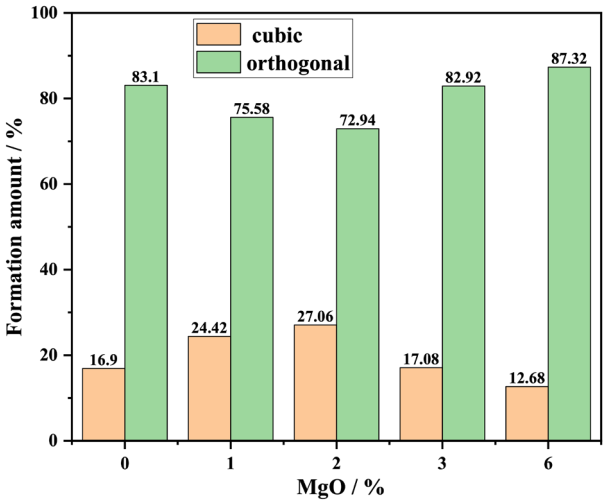

Figure 6. Formation of different $C_4A_3\$$ crystal structures with different MgO doping amounts.

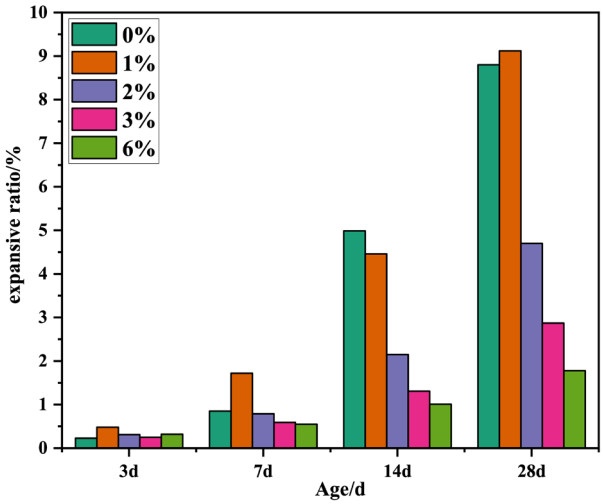

Figure 7. Hydration expansion rate of $C_4A_3\$$ with different MgO dosages at different maintenance ages.

to local stress. When the MgO content ranges from 2 to 6 %, the formation of cubic $C_4A_3\$$ decreases as the MgO content increases, likely due to changes in the coordination environment of Al^{3+} ions.

Effect of MgO content on hydration volumetric expansion rates

Figure 7 illustrates the hydration expansion rates of $C_4A_3\$$ with various MgO contents at different curing ages. When the curing time was less than 7 d, the expansion rates of the $C_4A_3\$$ phase samples with different MgO contents showed little variation. During this period, the expansion rate changes were primarily driven by the hydration of $C_4A_3\$$, with the influence of MgO hydration being minimal. In contrast to the large MgO particles commonly found in Portland cement, MgO in the $C_4A_3\$$ sintering system is more readily incorporated into the $C_4A_3\$$ phase structure. After 7 d, the expansion rates of the $C_4A_3\$$ phase samples exhibited significant changes, likely due to the MgO filling the lattice voids of the $C_4A_3\$$, which hindered the water penetration into the $C_4A_3\$$ crystal structure, thereby slowing the hydration process and affecting the expansion rate.

At low concentrations (less than 2 %), the hydration expansion of $C_4A_3\$$ is markedly reduced, suggesting that dissolved MgO plays a role in reducing cement expansion and enhancing hydration stability. However, when the MgO content increases to between 3 and 6 %, the reduction in expansion rate becomes less pronounced, suggesting that the amount of dissolved MgO in $C_4A_3\$$ is nearing saturation, with further increases in MgO content having a limited effect on expansion reduction.

The hydration process for f-MgO is slower, akin to the f-MgO in Portland cement. The f-MgO requires a longer time to hydrate and form magnesium hydroxide, which may lead to expansion, ultimately compromising the stability of the cementitious structure. Therefore, the improvement in the expansion rate is more pronounced for MgO dissolved in $C_4A_3\$$, whereas f-MgO, with its prolonged hydration time, carries a higher risk of expansion.

CONCLUSIONS

This study presents a detailed analysis of the sintering behaviour of $C_4A_3\$$ phase with various MgO contents under different sintering temperatures and holding times. The results are as follows:

The addition of MgO enhanced the formation of $C_4A_3\$$, particularly at a low sintering temperature (1250 °C) and a low MgO content (1 % MgO), where $C_4A_3\$$ began to form at a faster rate. The formation of $C_4A_3\$$ reached 70 %, which was only 10 % lower than the formation of $C_4A_3\$$ at the normal sintering temperature of 1350 °C.

In the $C_4A_3\$$ phase, MgO is incorporated as an interstitial solid solution rather than substitutional solid solution. Low MgO contents improve the hydration expansion rate of $C_4A_3\$$. At 2 % MgO, the hydration expansion rate of v decreases slightly, while higher MgO concentrations (3 – 6 %) show a progressively diminishing effect on the expansion, indicating that the MgO dissolved in the $C_4A_3\$$ structure effectively suppresses expansion and maintains the volume stability of the cement.

Acknowledgments

This work was supported by National Natural Science Foundation of China Regional Innovation and Development Joint Fund (U22A20126), Natural Science Foundations of China (52072149, 52002144), Science and Technology Innovation Support Plan for Young Researchers in Institutes of Higher Education in Shandong (2019KJA017), Taishan scholar program (tsqnz20221144, tsqn202211170) and the Center for international cooperation and disciplinary innovation ('111Center', No. D17001).

REFERENCES

1. Hu Y, Xiong L, Yan Y, Geng G. (2024): Performance of limestone calcined clay cement (LC3) incorporating low-grade marine clay. *Case Studies in Construction Materials, 20*, e3283. doi: 10.1016/j.cscm.2024.e03283
2. Ye P, Guo B, Qin H, Wang C, Li J, Chen Y, et al. (2024): Investigation of the properties and sustainability of modified biochar-doped cement-based composite. *Cement and Concrete Composites, 153*, 105684. doi: 10.1016/j.cemconcomp.2024.105684
3. Chen Y, Chaves Figueiredo S, Li Z, Chang Z, Jansen K, Çopuroğlu O, et al. (2020): Improving printability of limestone-calcined clay-based cementitious materials by using viscosity-modifying admixture. *Cement and Concrete Research, 132*, 106040. doi: 10.1016/j.cemconres.2020.106040
4. Song Q, Su J, Nie J, Li H, Hu Y, Chen Y, et al. (2021): The occurrence of MgO and its influence on properties of clinker and cement: A review. *Construction and Building Materials, 293*, 123494. doi: 10.1016/j.conbuildmat.2021.123494
5. Rehsi SS. (1983): Magnesium Oxide in Portland Cement. In: Editor, S.N. Ghosh. Advances in Cement Technology: Pergamon, 467-483. doi: 10.1016/B978-0-08-028670-9.50019-3
6. Amaral LF, Oliveira IR, Salomão R, Frollini E, Pandolfelli VC. (2010): Temperature and common-ion effect on magnesium oxide (MgO) hydration. C*eramics International, 36*(3), 1047-1054. doi: 10.1016/j.ceramint.2009.12.009
7. Elimbi A, Tchakoute HK, Njopwouo D. (2011): Effects of calcination temperature of kaolinite clays on the properties of geopolymer cements. *Construction and Building Materials, 25*(6), 2805-2812. doi: 10.1016/j.conbuildmat.2010.12.055
8. Berger S, Coumes CCD, Le Bescop P, Damidot D. (2011): Influence of a thermal cycle at early age on the hydration of calcium sulphoaluminate cements with variable gypsum contents. *Cement and Concrete Research, 41*(2), 149-160. doi: 10.1016/j.cemconres.2010.10.001
9. Yu S, He S, Chen H, Guo L. (2015): Effect of calcination temperature on oxidation state of cobalt in calcium cobaltite and relevant performance as intermediate-temperature solid oxide fuel cell cathodes. *Journal of Power Sources, 280*, 581-587. doi: 10.1016/j.jpowsour.2015.01.150
10. Wu S, Wang W, Ren C, Yao X, Yao Y, Zhang Q, et al. (2019): Calcination of calcium sulphoaluminate cement using flue gas desulfurization gypsum as whole calcium oxide source. *Construction and Building Materials, 228*, 116676. doi: 10.1016/j.conbuildmat.2019.116676
11. Padilla-Encinas P, Fernández-Carrasco L, Palomo A, Fernández-Jiménez A. (2022): Effect of alkalinity on early-age hydration in calcium sulfoaluminate clinker. *Cement and Concrete Research, 155*, 106781. doi: 10.1016/j.cemconres.2022.106781
12. Borštnar M, Daneu N, Dolenec S. (2020): Phase development and hydration kinetics of belite-calcium sulfoaluminate cements at different curing temperatures. *Ceramics International, 46*, 29421-29428. doi: 10.1016/j.ceramint.2020.05.029
13. Khaliq W, Khan HA. (2015): High temperature material properties of calcium aluminate cement concrete. *Construction and Building Materials, 94*, 475-487. doi: 10.1016/j.conbuildmat. 2015.07.023
14. Li L, Wang R, Zhang S. (2019): Effect of curing temperature and relative humidity on the hydrates and porosity of calcium sulfoaluminate cement. *Construction and Building Materials, 213*, 627-636. doi: 10.1016/j.conbuildmat.2019.04.044.
15. Yin C, Zong W, Wang S, Li G, Li Q, Lu L. (2011): Effect of MgO on Composition, Structure and Properties of Alite–Calcium Strontium Sulphoalminate Cement. *Journal of the Chinese Ceramic Society, 39*(1), 20-24.
16. Chen K, Yang CH, Wu F, Ye JX, Zhao SA, Xiang XB.

(2009): Study on Expansion of Cement-Based Material with Addition of Magnesium Oxide. *Materials Science Forum, 610-613*, 968-974. doi: 10.4028/www.scientific.net/MSF.610-613.968

17. Wang, Ai-juan, Song, Na, Rui, Bai, et al. (2017): Characterization of magnesium phosphate cement fabricated using pre-reacted magnesium oxide. *Journal of Alloys and Compounds, 696*, 560-565. doi: 10.1016/j.jallcom.2016.11.278
18. Abdel-Gawwad H. A. (2015): Retracted: Effect of reactive magnesium oxide on properties of alkali-activated slag-cement pastes. *Journal of Materials in Civil Engineering, 27*(8), 04014236. doi: 10.1061/(ASCE)MT.1943-5533.0001207
19. Jia, Yuan, Wang, Baomin, Zhenlin, Han, et al. (2016): Role of sodium hexametaphosphate in MgO/SiO_2 cement pastes. *Cement and Concrete Research, 89*, 63-71. doi: 10.1016/j.cemconres.2016.08.003
20. Sequeira L, Cantero B, Bravo JMC. (2023): The Influence of Recycled Cement, Fly Ash, and Magnesium Oxide on the Mechanical Performance of Sustainable Cementitious Materials. *Materials, 16*(7), 2760. doi: 10.3390/ma16072760
21. Sugama T, Kukacka LE. (1984). *Magnesium phosphate glass cements with ceramic-type properties* (No. US 4436555). Associated Universities, Inc., Upton, NY (United States).
22. Aziz MAE, Aleem SAE, Heikal M, Didamony HE. (2005): Hydration and durability of sulphate-resisting and slag cement blends in Caron's Lake water. *Cement and Concrete Research, 35*(8), 1592-1600. doi: 10.1016/j.cemconres.2004.06.038
23. Yu Z, Weiyang W, Qingfang L. (2023): The influence of reactive MgO on the hydration and carbonation performance of slag-rich cement system. *Journal of Building Engineering, 77*, 107477. doi: 10.1016/j.jobe.2023.107477
24. José N, Ahmed H, Miguel B, Luís E, Jorge DB. (2020): Magnesia (MgO) Production and Characterization, and Its Influence on the Performance of Cementitious Materials: A Review. *Materials, 13*(21), 4752. doi: 10.3390/ma13214752
25. Zhang Q., Deng M. (2009): Review on the expansion mechanism of cement paste mixed with Mgotype expansion agent. *Coll Mater Sci Eng Nanjing Uni Tech*, 111-115.
26. Mo LW, Deng M, Tang MS. (2009): Effect of Calcination Temperature on the Microstructure, Activity and Expansion of Mgo-Type Expansive Additive Used in Cement-Based Materials. *Key Engineering Materials, 400-402*, 169-174. doi: 10.4028/www.scientific.net/KEM.400-402.169
27. Mo L, Deng M, Wang A. (2012): Effects of MgO-based expansive additive on compensating the shrinkage of cement paste under non-wet curing conditions. *Cement and Concrete Composites, 34*(3), 377-383. doi: 10.1016/j.cemconcomp.2011.11.018
28. Wu F, Lv W, Li K, Kong L, Wang X, Chen H, et al. (2024): Chloride binding behavior and mechanism of phosphoaluminate cement clinker and its hydration products. *Construction and Building Materials, 438*, 137138. doi: 10.1016/j.conbuildmat.2024.137138
29. Yu L, Bi H, Wang Z, Wu F, Hou P, Wang S, et al. (2023): Feasibility of using iron-rich phosphoaluminate cement to prepare anti-corrosive coatings for rebars. *Construction and Building Materials, 401*, 132736. doi: 10.1016/j.conbuildmat.2023.132736
30. Bi H, Zhang W, Xu X, Ming A, Shen Y, Wang S, et al. (2021): Chloride binding and transport characteristic of phosphoaluminate cement-based marine sand coating subjected to marine environment. C*onstruction and Building Materials, 281*, 122505. doi: 10.1016/j.conbuildmat.2021.122505
31. Wang Z, Xue L, Huang Y, Yu L, Wu F, Wang S. (2024): Effects of slag on mechanical and microstructural properties of iron-rich phosphoaluminate cement subjected to high temperature oil well environment. *Geoenergy Science and Engineering, 240*, 213067. doi: 10.1016/j.geoen.2024.213067
32. Mohamed LK, Shaban SA, El-Kady FY. (2010): Effect of Calcination Temperature on the Characterization of Spent Catalyst. *Petroleum Science and Technology, 28*(3), 322-330. doi: 10.1080/10916460903058103
33. Martin É, Azzi M, Salishchev GA, Szpunar J. (2010): Influence of microstructure and texture on the corrosion and tribocorrosion behavior of Ti–6Al–4V. *Tribology International, 43*(5), 918-924. doi: 10.1016/j.triboint.2009.12.055
34. Rossé P, Loizeau JL. (2003): Use of single particle counters for the determination of the number and size distribution of colloids in natural surface waters. *Colloids and Surfaces A Physicochemical and Engineering Aspects, 217*(1), 109-120. doi: 10.1016/S0927-7757(02)00565-4
35. Lv W, Zhang Y, Ren X, Feng Y, Wang S, Zhao P. (2023): Effect of strontium slag on early hydration and mechanical properties of belite-$C_4A_3\$$ cement. *Materials Today Communications, 36*, 106572. doi: 10.1016/j.mtcomm.2023.106572
36. Lingling X, Nanru Y, Baiqian Z. (1995): Effect of MgO on the hydration properties of $C_4A_3\$$. *Journal of the Chinese Ceramic Society, 1995*(2), 206-210.